Phosphorylation of FE65 Ser^{610} by serum- and glucocorticoid-induced kinase 1 modulates Alzheimer's disease amyloid precursor protein processing

Wan Ning Vanessa Chow*, Jacky Chi Ki Ngo*, Wen Li*, Yu Wai Chen†, Ka Ming Vincent Tam*, Ho Yin Edwin Chan*, Christopher C.J. Miller‡ and Kwok-Fai Lau*[1]

*School of Life Sciences, Faculty of Science, The Chinese University of Hong Kong, Shatin, N.T., Hong Kong SAR
†King's College London, Randall Division of Cell and Molecular Biophysics, London SE1 1UL, U.K.
‡Department of Basic and Clinical Neuroscience, Institute of Psychiatry, Psychology & Neuroscience, King's College London, London SE5 8AF, U.K.

Alzheimer's disease (AD) is a fatal neurodegenerative disease affecting 36 million people worldwide. Genetic and biochemical research indicate that the excessive generation of amyloid-β peptide (Aβ) from amyloid precursor protein (APP), is a major part of AD pathogenesis. FE65 is a brain-enriched adaptor protein that binds to APP. However, the role of FE65 in APP processing and the mechanisms that regulate binding of FE65 to APP are not fully understood. In the present study, we show that serum- and glucocorticoid-induced kinase 1 (SGK1) phosphorylates FE65 on Ser^{610} and that this phosphorylation attenuates FE65 binding to APP. We also show that FE65 promotes amyloidogenic processing of APP and that FE65 Ser^{610} phosphorylation inhibits this effect. Furthermore, we found that the effect of FE65 Ser^{610} phosphorylation on APP processing is linked to a role of FE65 in metabolic turnover of APP via the proteasome. Thus FE65 influences APP degradation via the proteasome and phosphorylation of FE65 Ser^{610} by SGK1 regulates binding of FE65 to APP, APP turnover and processing.

Key words: amyloid-β peptide, Alzheimer's disease, amyloid precursor protein (APP), FE65, serum- and glucocorticoid-induced kinase 1 (SGK1), protein degradation.

INTRODUCTION

Alzheimer's disease (AD) is a progressive neurodegenerative disease affecting 36 million people worldwide. Despite its long history of discovery, effective treatment against the disease is still lacking [1]. Previous genetic, biochemical and behavioural research shed light on the importance of accumulation of amyloid β peptide (Aβ) in AD pathogenesis [2]. Aβ is a proteolytic cleavage product of amyloid precursor protein (APP), a transmembrane protein known to be a substrate of regulated intramembrane proteolysis (RIP) involving the combined actions of α-secretase, β-secretase and γ-secretase. Under normal circumstances, APP would mainly follow the non-amyloidogenic pathway which does not produce the toxic Aβ. In AD patients, however, more APP would follow the amyloidogenic pathway in which APP is cleaved by β- and γ-secretase sequentially, generating Aβ which eventually leads to deposition of extracellular amyloid plaque [2,3]. In this regard, understanding how proteolytic cleavage of APP is regulated emerges as a critical field of research in developing therapeutic intervention against AD.

Although the mechanisms are still not fully understood, evidence shows that APP-interacting proteins, including APP intracellular domain (AICD) interactors, play essential roles in regulating APP processing [3,4]. It is generally believed that AICD serves as a docking site for a number of intracellular proteins including FE65 and enables the formation of different protein complexes that modulate APP processing [3,5]. FE65 is a brain-enriched adaptor protein with abundant expression in hippocampus, the region which is severely affected in AD [6]. It possesses three conserved protein interaction domains, namely an N-terminal WW domain and two C-terminal phosphotyrosine-binding (PTB) domains, which allow the formation of multi-molecular complexes. It is well characterized that through its second PTB domain (PTB2), FE65 physically binds to the YENPTY motif of APP [3,7]. In recent years, an increasing body of evidence suggests that FE65 modulates APP processing and that APP–FE65 interaction is essential to the alteration in APP processing [8–14]. However, conflicting findings are reported for the effect of FE65 on APP processing [8–10,15]. It is proposed that such contradictory observations are partly due to differences in the phosphorylation status of FE65 [3].

Phosphorylation is a common post-translational modification that regulates protein–protein interaction. In fact, we have previously shown that FE65–Dexras1 interaction is modulated by FE65 Tyr^{547} phosphorylation [16]. Therefore, phosphorylation of FE65 clearly plays an essential role in regulating the interaction between FE65 and its interactors. Moreover, FE65 phosphorylation, including Tyr^{547} and Ser^{228}, has been found to alter FE65–APP-mediated gene transcription [17]. These findings highlight the biological relevance of FE65 phosphorylation. In the present study, we investigated the role of phosphorylation of FE65 Ser^{610}, a residue that lies in the interaction interface of APP–FE65. Using a commercial kinase finder approach (ProQinase),

Abbreviations: 3-MA, 3-methyladenine; aa, amino acid; AD, Alzheimer's disease; AICD, APP intracellular domain; ApoE, apolipoprotein E; APP, amyloid precursor protein; APPc, APP cytosolic tail; Aβ, amyloid-β peptide; BACE1, β-site amyloid precusor protein cleaving enzyme 1; CHO, Chinese hamster ovary; CHX, cycloheximide; CTF, C-terminal fragment; DS, Down's syndrome; ER, endoplasmic reticulum; FBL2, F-box and leucine-rich repeat protein 2; HEK293, human embryonic kidney 293; IPs, immunoprecipitates; LRP1, low-density lipoprotein receptor-related protein; pSer, phosphoserine; PTB domain, phosphotyrosine-binding domain; RIPA, radioimmunoprecipitation assay buffer; SGK1, serum- and glucocorticoid-induced kinase 1; SGK1-CA, constitutively active SGK1 mutant; TGFβ, transforming growth factor β; UPS, ubiquitin-proteasome system; VLDLR, very low density lipoprotein receptor; WT, wild-type.

[1] To whom correspondence should be addressed (email kflau@cuhk.edu.hk).

© 2015 Authors; published by Portland Press Limited

serum- and glucocorticoid-induced kinase 1 (SGK1) was found to be a candidate kinase for FE65 Ser^{610}. Moreover, we found that phosphorylation of FE65 Ser^{610} by SGK1 markedly diminishes APP–FE65 interaction. It follows that when FE65 Ser^{610} is phosphorylated, the enhancing effect of FE65 on APP processing and Aβ liberation is attenuated. We also found that the phosphorylation state of Ser^{610} of FE65 regulates the turnover of APP, which explains, at least in part, why APP processing is affected. Our study revealed a novel molecular mechanism that governs APP processing and Aβ generation.

MATERIALS AND METHODS

Cell culture and transfection

Chinese hamster ovary (CHO) cells were cultured in Ham's F12. Human embryonic kidney 293 (HEK293) and COS-7 cells were maintained in Dulbecco's Modified Eagle Medium (DMEM) low glucose. All culture media are supplemented with 10 % (v/v) FBS. Plasmid transfection was performed using X-tremeGENE 9 (Roche) or X-tremeGENE HP (Roche) according to the manufacturer's instructions. For knockdown experiments, siRNAs purchased from Dharmacon, Thermo Scientific were transfected to cells using Lipofectamine RNAiMAX (Invitrogen). The effect of the ubiquitin–proteasome system and autophagy on APP degradation was evaluated by treating cells with 2.5 μM MG132 (Merck Chemicals) for 16 h and 5 mM 3-methyladenine (3-MA; Santa Cruz) for 12 h respectively.

Plasmids

His-tagged human SGK1 plasmid was a kind gift of Professor David Pearce (University of California, San Francisco). Constitutively active SGK1 mutant (SGK1-CA) was prepared by mutating Ser^{422} to aspartate (S422D) by Quikchange II site-directed mutagenesis. Mammalian expression constructs of human APP_{695} isoform, β-site amyloid precusor protein cleaving enzyme 1 (BACE1) and myc-tagged FE65 were as described [18–20]. Point mutations on Ser^{610} of FE65 were introduced by Quikchange II site-directed mutagenesis. GST–APPc [APP cytosolic tail; amino acid (aa) 599-695] bacterial expression plasmid was as previously described [18]. GST–$FE65_{598\text{-}619}$ WT (wild-type) and GST–$FE65_{598\text{-}619}$ S610A were cloned into EcoRI and XhoI sites of pGEX-6p-1 by annealed oligo cloning. The APP–GAL4 plasmid which encodes human APP_{695} followed by full-length GAL4 yeast transcription factor was described previously [21]. The GAL4-dependent firefly luciferase plasmid pFR-Luc and the transfection efficiency control reporter *Renilla* luciferase plasmid phRL-TK were purchased from Stratagene and Promega respectively.

Antibodies

Myc-tagged FE65 was detected with anti-myc 9B11 antibody (Cell Signaling Technology) or E20 anti-FE65 antibody (Santa Cruz). The same antibody was also used to detect endogenous FE65 in knockdown experiments. APP was detected with a rabbit anti-APP antibody as described previously [22]. DM1A anti-α-tubulin antibody and anti-FBL2 (F-box and leucine-rich repeat protein 2) antibody were obtained from Santa Cruz. 9B21 anti-BACE1 antibody was as described [20]. P4D1 anti-ubiquitin antibody and rabbit polyclonal anti-p62 antibody were purchased from Cell Signaling Technology. His-tagged SGK1 was immunoprecipitated with anti-His antibody (Proteintech). Serine-phosphorylated proteins were immunoprecipitated by an anti-phosphoserine (pSer) antibody (Abcam). 22C11 anti-APP antibody (Millipore) and a rabbit anti-FE65 antibody as described [16] were used in immunofluorescence staining.

GST pull-down assay

GST pull-down assay was performed as described previously [23]. In brief, GST and GST–APPc fusion protein were expressed in *Escherichia coli* BL21 and immobilized on glutathione sepharose 4B (GE Healthcare) according to the manufacturer's instructions. FE65 S610A and FE65 S610D were overexpressed in CHO cells. Transfected cell lysates were prepared in ice-cold cell lysis buffer composed of 50 mM Tris/HCl, pH 7.5, 150 mM NaCl, 1 mM EDTA, 1 % (v/v) Triton X-100 and Complete™ proteinase inhibitor (Roche) as described [16]. The immobilized GST and GST–APPc baits were allowed to incubate with the transfected cell lysates at 4 °C for 3 h. The baits were washed with ice-cold lysis buffer three times at the end of incubation and the captured proteins were resolved on SDS/PAGE. FE65 was immunoblotted with 9B11 anti-myc antibody against the C-terminal myc tag.

Co-immunoprecipitation

CHO cells were transfected with APP + either myc-tagged FE65 S610A or S610D. Cells were harvested in ice-cold cell lysis buffer as detailed above. Myc-tagged FE65 was immunoprecipitated from cell lysate using 9B11 anti-myc antibody and subsequently captured by Protein A-agarose (Sigma). The immunoprecipitates were washed three times with ice-cold lysis buffer afterwards. Proteins in the immunoprecipitates were subjected to analysis by SDS/PAGE and Western blotting. APP and myc-tagged FE65 were detected by an anti-APP antibody and 9B11 anti-myc antibody respectively. Co-immunoprecitation of APP and FE65 in the absence or presence of SGK1-CA was performed similarly.

Kinase Finder radiometric protein kinase assays

Kinase Finder radiometric protein kinase assay was performed by ProQinase. In brief, a biotinylated peptide of FE65 (CRVRFLSFLAVGR; residues 604–616) was incubated with various kinases from a panel of 190 recombinant serine/threonine kinases and reaction cocktails (60 mM HEPES/NaOH, pH 7.5, 3 mM $MgCl_2$, 3 mM $MnCl_2$, 3 μM sodium orthovanadate, 1.2 mM DTT, 50 μg/ml PEG 20000, 1 μM [γ-^{33}P]-ATP) at 30 °C for 60 min. The reactions were terminated by adding an appropriate amount of stop solution (4.7 M NaCl, 35 mM EDTA) and then transferred to streptavidin-coated 96-well FlashPlate PLUS plates (PerkinElmer). The plates were incubated at room temperature for 30 min and then washed three times with 0.9 % (w/v) NaCl. Radioactive ^{33}P signals were measured by a microplate scintillation counter.

In vivo phosphorylation assay

Cells transfected with myc-tagged FE65 with or without SGK1-CA were harvested in ice-cold RIPA (radioimmunoprecipitation assay) buffer composed of 50 mM Tris, pH 7.6, 150 mM NaCl, 1 mM EDTA, 1 % (w/v) sodium deoxycholate, 0.1 % (w/v) SDS, 1 % (v/v) Triton X-100, supplemented with 0.5 mM sodium orthovanadate, 30 mM NaF and Complete™ proteinase inhibitor (Roche). Serine-phosphorylated proteins were immunoprecipitated from cell lysate using anti-pSer antibody (Abcam) and subsequently captured by protein A-agarose (Sigma). The immunoprecipitates were washed three times with ice-cold RIPA buffer and subjected to analysis by

© 2015 Authors; published by Portland Press Limited

SDS/PAGE and Western blotting. Myc-tagged FE65 and His-tagged SGK1-CA were detected by 9B11 anti-myc antibody and an anti-His antibody respectively.

In vitro kinase assay

SGK1-CA was immunoprecipitated from transfected CHO cell lysate using anti-His antibody followed by antibody capturing with protein A-agarose (Sigma). The immunoprecipitates were washed two times with ice-cold lysis buffer followed by 1× kinase buffer (60 mM HEPES/NaOH pH 7.5, 3 mM $MgCl_2$, 3 mM $MnCl_2$, 1.2 mM DTT, 3 μM sodium orthovanadate) once. The immunoprecipitates bound protein A-Agarose beads were resuspended in 1× kinase buffer and used immediately for kinase assay. Each reaction tube was composed of 10 μl of immunoprecipitated kinase, 0.5 μg of substrate and 0.5 μl of 3000 Ci/mmol 5 μCi/μl [γ-^{32}P]-ATP to a total volume of 20 μl. The reaction mixture were incubated at 30 °C for 30 min, resolved on SDS/PAGE and exposed to an autoradiogram.

Preparation of simulation models

The crystal structure of FE65–PTB2 (PDBID 3DXC) chain A was used as the starting structure for simulation of the free apo protein with Ser^{610} (PTB2-S610). After the MD simulation, the most representative structure was used as the reference model for the preparation of the other two models. The PTB2–S610D model was created in Coot [24] employing the built-in rotamer library [25]. The model of PTB2 with phosphorylated Ser^{610} (PTB2–pS610) was prepared with the SIDEpro server [26], with all atoms fixed except for Cβ and Oγ of Ser^{610}. The phosphorylated serine side chain is assumed to be not protonated and carries a charge of -2.

MD

MD was performed with the program GROMACS 4.5.5 [27] employing the GROMOS 54A7 force field which includes phosphorylated residues [28], maintained by the Vienna-PTM server [29]. The initial models were immersed in an octahedral solvent box with 1.0 nm thick edges and with SPC water model. Sodium and chloride ions were added to a physiological concentration of 0.15 M and to neutralize the protein overall charges. For all runs, all bond lengths were constrained by using the LINCS algorithm [30] and the simulation step size was 2 fs. Particle mesh Ewald summation was employed for electrostatic interaction calculations, with a cut-off radius of 0.9 nm. A cut-off radius of 1.4 nm was applied to van der Waals interactions. The list of neighbours of each atom, with a cut-off radius of 0.9 nm, was updated every 10 steps. The solvated model was first allowed to relax by unrestrained energy minimization (steepest descent) to reach a target maximum force of 1000.0 kJ mol^{-1}·nm^{-1}. Next, the system temperature was raised to 300 K over 100 ps, using the velocity-rescaling thermostat (NVT [substance (N), volume (V) and temperature (T)] ensemble), with a positional restraint of 1000.0 kJ mol^{-1}·nm^{-2} applied to all protein atoms. Then the system pressure was adjusted to 1 bar for 400 ps, using the Berendson barostat (NPT [substance (N), pressure (P) and temperature (T)] ensemble). During this stage, the positional restraint was progressively reduced from 1000.0 to 0.1 kJ mol^{-1}·nm^{-2} over eight steps of 100 ps each. The production phase of each system comprises of 10 ns unstrained MD simulations using the leapfrog algorithm. The structures and energies were saved every 10 ps.

Analysis

RMSD calculations were performed using VMD software [31]. The structures were aligned using all Cα atoms, with the co-ordinates of the most representative structure of the FE65–PTB2 Ser^{610} simulation as the reference.

Indirect immunofluorescence

Transfected COS-7 cells grown on glass coverslips were fixed and processed, as previously described [32]. APP was detected with 22C11 anti-APP antibody whereas FE65 was detected with a rabbit anti-FE65 antibody as described [16]. The primary antibodies were visualized by Alexa Fluor® 488 and 594 secondary antibodies (Invitrogen). DAPI was purchased from Sigma for nuclei staining. Images were captured with an inverted fluorescence microscope (Olympus) and the subcellular localization of FE65 was quantified.

APP–GAL4 luciferase reporter assay

Cells were transfected with FE65/FE65 S610A/FE65 S610D together with APP–GAL4, pFR-Luc and phRL-TK. Forty-eight hours post-transfection, luciferase activity was assayed using a Dual-Glo luciferase assay system (Promega) according to the manufacturer's instructions. The firefly and *Renilla* luciferase activities were measured by a luminometer (Wallace) and the ratio of firefly luciferase activity to *Renilla* luciferase activity is denoted as relative luciferase activity.

Tris-tricine SDS/PAGE analysis for APP CTFs

APP CTFs (C-terminal fragments) were resolved on 16 % Tris-tricine SDS/PAGE as described previously followed by Western blot analysis [33]. A rabbit anti-APP antibody that was raised against the last 21 aa residues of APP was used to detect for the CTFs [22,33].

Aβ ELISA assay

Human Aβ 1–42 secreted into the cell culture medium was assayed with a High Sensitivity Human Amyloid β42 ELISA kit (Millipore) according to the manufacturer's instructions. In brief, CHO cells were transfected with APP + indicated constructs using X-tremeGENE HP (Roche) to achieve high transfection efficiency. Forty-eight hours post-transfection, cell culture medium was aspirated and replaced with fresh culture medium. Seven hours afterwards, the medium was collected and the amount of Aβ 1–42 secreted within this period was assayed with the ELISA kit.

Cycloheximide chase assay

Transfected cells were treated with 10 μg/ml cycloheximide (CHX) 48 h post-transfection for 0, 2, 4 and 8 h. At the end of CHX treatment, cells were lysed in SDS sample buffer to obtain protein lysates for Western blot analysis. α-Tubulin was used as loading control. The relative amount of APP was quantified using ImageJ and plotted as percentage of APP at 0 h for each transfection.

Statistical analyses

Statistical analyses were performed using unpaired *t* test or one-way ANOVA test. Significance between different treatments is indicated as $*P < 0.0001$, $**P < 0.01$, $***P < 0.05$, ns–$P > 0.05$.

© 2015 Authors; published by Portland Press Limited

RESULTS

Phosphorylation of FE65 Ser^{610} interferes with APP–FE65 interaction

According to the crystal structure of the AICD-C32$_{aa\ 664\text{-}695}$–FE65–PTB2 complex, FE65 Ser^{610} is found to lie in its interaction interface [34]. Intriguingly, such a residue is reported to be phosphorylated in an FE65 isoform from mass spectrometric analysis [35]. Therefore, we investigated whether FE65 Ser^{610} phosphorylation alters FE65–APP interaction. To test this, GST pull-down assay was performed using bacterially expressed GST–APPc (aa 599–695) fusion protein as bait to pull down CHO cell lysates transiently transfected with dephosphomimetic mutant FE65 S610A or phosphomimetic mutant FE65 S610D (Figure 1A). FE65 S610A was found to bind strongly to APPc, but the binding of FE65 S610D to APPc is substantially weaker, indicating that Ser^{610} is a critical aa of APP–FE65 interaction. In complement to GST pull-down assay, co-immunoprecipitation was performed by co-transfecting APP with either myc-tagged FE65 S610A or S610D to CHO cells. Western blotting revealed that a greater amount of APP co-immunoprecipitated with FE65 S610A than with FE65 S610D (Figure 1B). This provides further evidence that phosphorylation of FE65 Ser^{610} attenuates APP–FE65 interaction.

To identify FE65 Ser^{610} kinases, we employed the commercial Kinase Finder radiometric protein kinase assay (ProQinase) which is a radiometric kinase assay for a panel of 190 serine/threonine kinases. The results suggested that SGK1 is a putative FE65 Ser^{610} kinase (Supplementary Table S1). Intriguingly, the aa sequence around FE65 Ser^{610} is found to be the SGK1 targeting consensus (R-X-R-X-X-S/T-φ; φ = hydrophobic residue) [36,37]. To test if SGK1 alters the phosphorylation status of FE65 *in vivo*, cells were transfected with FE65 or FE65 + SGK1-CA and immunoprecipitated with pSer antibody. We found that an increased amount of FE65 was detected in the immunoprecipitate from cells co-transfected with SGK1 (Figure 1C). The result revealed that SGK1 enhances serine phosphorylation of FE65. In order to validate FE65 Ser^{610} is the target residue of SGK1, bacterially expressed GST–FE65$_{598\text{-}619}$ WT and GST–FE65$_{598\text{-}619}$ S610A were incubated with SGK1-CA immunoprecipitated from transfected cell lysate together with [γ-^{32}P]-ATP for 30 min at 30 °C. The reaction mixture was resolved on SDS/PAGE and exposed to an autoradiogram. As shown in Figure 1(D), SGK1 induces phosphorylation on WT but not on S610A mutant. We hereby showed that SGK1 phosphorylates FE65 at Ser^{610} directly.

Next, we investigated whether SGK1 interferes with APP–FE65 interaction. To do this, co-immunoprecipitation was performed from cells co-transfected with APP + FE65 or APP + FE65 + SGK1-CA. FE65 was immunoprecipitated by an anti-myc antibody and the immunocomplex was analysed for APP. As shown in Figure 1(E), less APP co-immunoprecipitated with FE65 in the presence of SGK1-CA, indicating that SGK1-CA weakens the interaction between APP and FE65.

A model of Ser^{610}-phosphorylated FE65 PTB2 domain reveals the mechanism of disruption of APP binding

To understand the molecular basis of how Ser^{610} phosphorylation affects the binding of FE65 to APP, we constructed two models of the FE65 PTB2 domain, with residue Ser^{610} modified to pSer^{610} or changed to aspartate (S610D). The apo-FE65 PTB2 structure and its two variants were studied by MD simulations. We then compared the structural stability of the whole domain as well as the local region where Ser^{610} is located (aa 601–614) in the native and modified PTB2 models by computing the RMSD of the Cα atoms from their initial positions. Figure 2(A) shows that the RMSD of the Cα atoms within either the whole PTB2 domain (top panel) or the local region surrounding residue 610 (bottom panel) of both modified models remained steady in the stable phase of the simulations and did not deviate much from those of the native model.

The slightly higher local deviation shown by the S610D mutant might be due to the aspartate side chain having an sp^2 Cγ atom, which is sterically different from the sp^3 Oγ atom of serine (and pSer^{610}), leading to some adaptation of the neighbours. Nevertheless, this small deviation of 1.0–1.2 Å (1 Å = 0.1 nm) is well within normal co-ordinate variations observed in different experimental structures.

The simulation results indicate that the phosphorylation of Ser^{610} did not affect the local conformation nor the overall stability of the PTB domain, suggesting that the loss of APP binding is not caused by major conformational change in the phosphorylated FE65 PTB2 structure.

Since Ser^{610} locates at the binding interface between FE65 and APP, the conformation of Ser^{610} could play a key role in determining the binding of APP. We therefore tried to identify the preferred χ_1 rotamer configuration (N-Cα-Cβ-X dihedral; rotation along Cα-Cβ bond) of Ser^{610} in the MD simulation trajectories. During the simulations, the side chain of Ser^{610} was equally populated in the p (plus, $\chi_1 = 60^o$) and t (trans, $\chi_1 = 180^o$) rotamer conformations, with a slightly lower population in the m (minus, $\chi_1 = -60^o$) conformation (nomenclature according to the rotamer library by Lovell et al. [25]; Figure 2B), suggesting that the side chain of Ser^{610} could equally adopt any of these three conformations and allows APP to bind due to its small size. This observation agreed well with the FE65–APP complex crystal structures (PDB ID: 3DXC or 3DXD) where Ser^{610} assumes the p-conformation upon binding of APP, despite being slightly strained ($\chi_1 = 42°$ or 44°) due to packing against the side chain of Tyr^{687} of APP at the binding interface.

On the other hand, when Ser^{610} was phosphorylated, the larger side chain preferentially adopted the t-rotamer conformation and only occasionally changed to -100^o, whereas both p- and m-conformations were prohibited due to steric hindrance from the strand β6 and the loop between strand β1 and helix α2 (Figure 2C). As a result, the side chain pointed out into the solvent and might disrupt APP binding due to steric clash with Tyr^{687} of APP (Figure 2C). Similar observation was made with the S610D mutant where its side chain predominantly adopted the t-conformation (Figure 2D). Our MD simulation results therefore provided a convincing explanation of how phosphorylation of Ser^{610} or its mutation to aspartate may disrupt APP binding.

FE65 S610D does not co-localize with APP

An important implication of APP–FE65 interaction is that APP serves as a cytosolic tethering site of FE65 and prevents FE65 nuclear localization [38]. As phosphorylation of FE65 Ser^{610} precludes binding of FE65 to APP, we wondered if the phosphorylation alters FE65 subcellular localization. Immunofluorescence staining was performed using COS-7 cells transiently transfected with either APP + FE65, APP + FE65 S610A or APP + FE65 S610D. Consistent with a previous report [38], APP and FE65 were found to co-localize in the perinuclear region (Figures 3A–3D). In the present study, we demonstrated that FE65 S610A is also tethered to the perinuclear region by APP (Figures 3E–3H). On the other hand, in the majority of cells (72 % of cell population), FE65 S610D, which is unable to bind

© 2015 Authors; published by Portland Press Limited

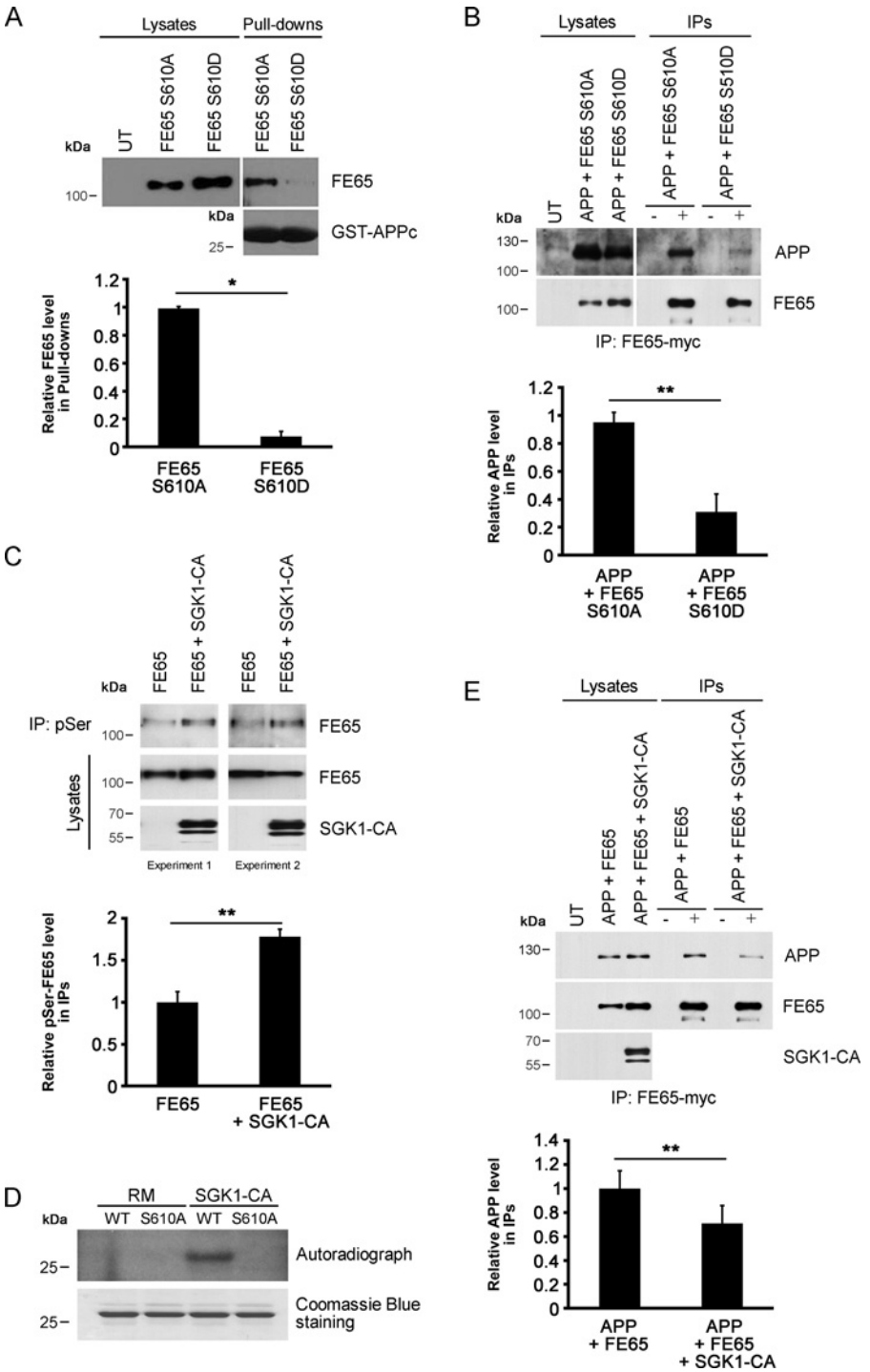

Figure 1 Phosphorylation of FE65 Ser^{610} by SGK1 suppresses APP–FE65 interaction

(**A**) Bacterially expressed GST–APPc was used as bait for GST pull-down assay from FE65 S610A or S610D-transfected cell lysate. FE65 S610A and S610D were detected by 9B11 anti-myc antibody against the C-terminal myc tag. Bottom panel shows Coomassie Blue staining of GST–APPc bait used. (**B**) Co-immunoprecipitation was performed from CHO cells transfected with APP + FE65 S610A or FE65 S610D using anti-myc antibody. APP interacts with FE65 S610A but not FE65 S610D. (**C**) Serine-phosphorylated proteins were immunoprecipitated from FE65 or FE65 + SGK1-CA transfected cell lysates. The level of FE65 in the immunoprecipitates (IPs) and the input lysates was detected by anti-myc antibody. SGK1 enhances serine phosphorylation of FE65 in cells. (**D**) Bacterially expressed GST–FE65$_{598\text{-}619}$ WT or S610A were incubated with SGK1-CA immunoprecipitated from transfected cell lysate together with [γ-^{32}P]-ATP for 30 min at 30°C. RM is the reaction mix only without kinase. Upper panel: autoradiograph; Lower panel: Coomassie Blue staining. SGK1 phosphorylates FE65 at Ser^{610}. (**E**) Co-immunoprecipitation was performed from CHO cells transfected with APP + FE65 or APP + FE65 + SGK1-CA using anti-myc antibody. APP was detected with anti-APP antibody whereas FE65 was detected by an anti-myc antibody. SGK1 interferes with APP–FE65 interaction. (−) and (+) in (**B**) and (**E**) refer to the absence or presence of antibody in the IPs. Amount of FE65/FE65 S610A/FE65 S610D DNA used in transfections was adjusted to ensure equal amount of input lysate in the interaction assays for fair comparison. UT indicates untransfected. FE65 and APP levels were measured by a densitometer (Bio-Rad) and analysed by ImageJ. Data for graphs in (**A**–**C**) and (**E**) were obtained from three independent experiments ($n = 3$). *$P < 0.0001$; **$P < 0.01$. Results are means ± S.D.

© 2015 Authors; published by Portland Press Limited

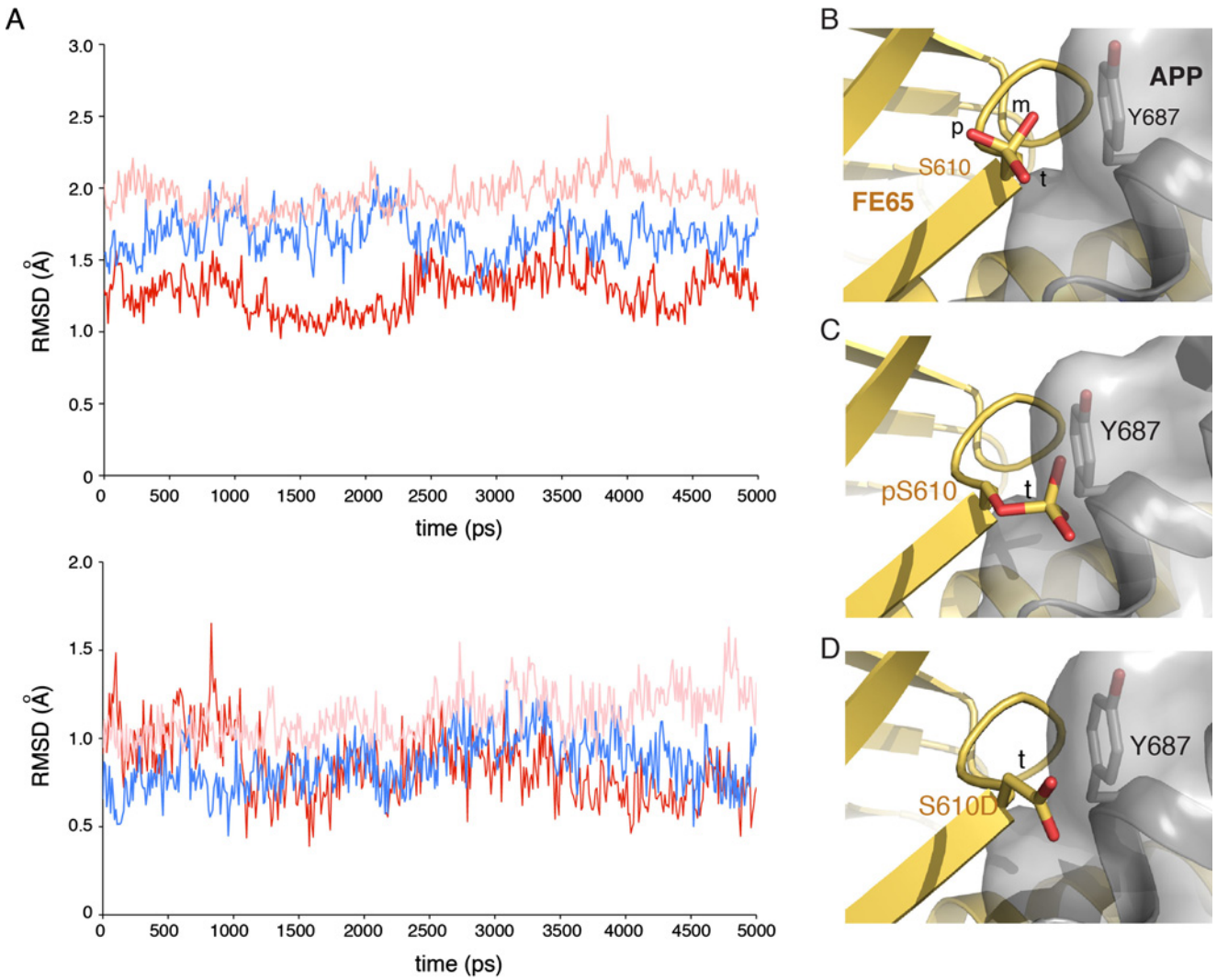

Figure 2 Phosphorylation of Ser^{610} disrupts the binding of APP

(**A**) Structural comparison of the FE65 PTB2 domains (top panel) and local regions neighbouring Ser^{610} (bottom panel) relative to the reference structure: RMSD of Cα atoms of Ser^{610} (red), pSer^{610} (blue) model and S610D (pink) mutant. (**B**) Ser^{610} of FE65 can adopt all three (p, m and t) rotamer conformations during the MD simulation. All conformations of the small side chain can accommodate Tyr^{687} of APP (grey). (**C**) Phosphorylated Ser^{610} and (**D**) S610D mutant favour the t-conformation that clashes with Tyr^{687} and disrupts APP binding.

to APP, retains in the nucleus (Figures 3I–3L). Quantification of subcellular localization of FE65 is shown in Figure 3(M).

Phosphorylation of FE65 Ser^{610} abolishes the effect of FE65 on APP processing

Aberrant processing of APP would result in excessive Aβ generation and the process is known to be modulated by a number of APP-interacting proteins including FE65. As phosphorylation of FE65 Ser^{610} prevents APP–FE65 interaction, we speculated that this phosphorylation event might be involved in the regulation of FE65-mediated APP processing. To address this issue, we first employed an APP–GAL4 reporter system to evaluate the effect of FE65 Ser^{610} phosphorylation on γ-secretase-mediated APP cleavage. In this system, the full-length yeast transcription factor GAL4 is fused to the C-terminus of APP (APP–GAL4). When cleaved by γ-secretase, the AICD fused with GAL4 would be released from the membrane-tethered part of APP and translocate to the nucleus to activate GAL4-dependent firefly luciferase transcription. As shown in Figure 4(A), overexpression of FE65 and FE65 S610A enhances γ-secretase-mediated APP processing, whereas FE65 S610D is unable to stimulate APP cleavage.

Next, the cleavage pattern of APP was studied by immunoblotting for CTFs. As reviewed in [2], β-secretase BACE1 cleaves APP at two sites, aa 1 or 11 of Aβ, generating CTFβ and CTFβ' respectively, whereas α-secretase cleaves APP at aa 17 of Aβ, generating CTFα. Full-length Aβ can only be produced when APP is cleaved by BACE1 at aa 1 that gives rise to CTFβ. We therefore analysed the CTFs pattern to evaluate the effect of FE65 Ser^{610} phosphorylation on α/β-secretase-mediated cleavage. As shown in Figure 4(B), overexpression of FE65 or FE65 S610A in APP + BACE1 co-transfected cells increases APP holoprotein, CTFβ and CTFβ' levels, indicating that both FE65 and FE65 S610A promote APP β-cleavage, possibly through

© 2015 Authors; published by Portland Press Limited

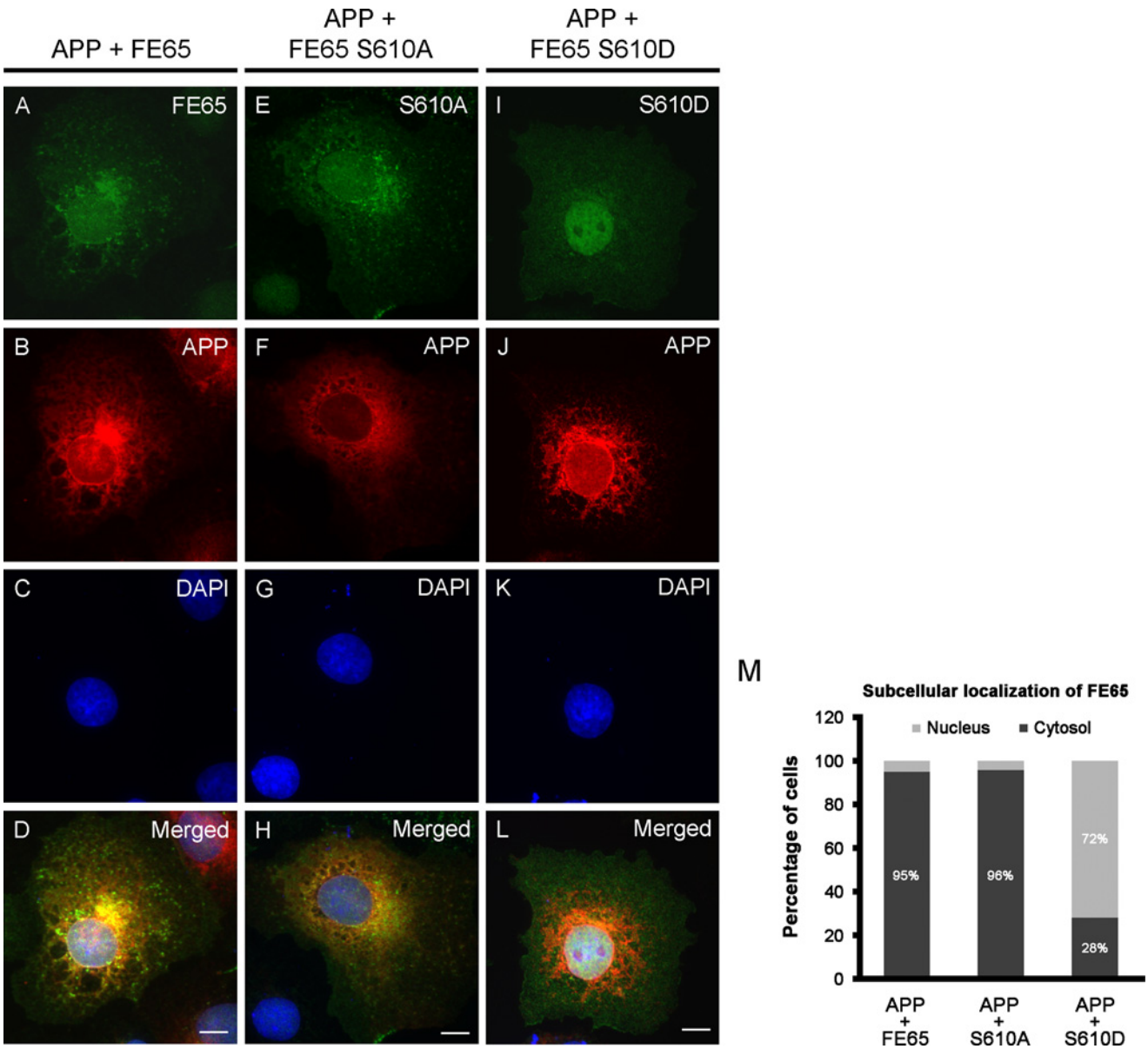

Figure 3 APP and FE65 S610A co-localize in the perinuclear region

Immunofluorescence staining of COS-7 cells transfected with APP + FE65 (**A**–**D**), APP + FE65 S610A (**E**–**H**) and APP + FE65 S610D (**I**–**L**). (**A**, **E** and **I**) Labelled for FE65; (**B**, **F** and **J**) labelled for APP; (**C**, **G** and **K**) labelled for nucleus by DAPI; (**D**, **H** and **L**) Overlaid images. Scale bars are 10 μm. (**M**) Subcellular localization of FE65 was quantified and expressed as percentage of cells with cytosolic and nuclear localization. $n = 20$. Three independent experiments were performed with similar results.

stabilization of APP holoprotein (to be discussed in detail below). However, such effect is lost when FE65 S610D was overexpressed instead.

As FE65 S610A but not FE65 S610D was found to promote APP β- and γ-cleavage, we investigated whether Aβ liberation was affected by FE65 Ser^{610} phosphorylation. To do this, APP + FE65/FE65 S610A/FE65 S610D were co-transfected into CHO cells and the amount of secreted Aβ was measured by Aβ ELISA kit. In line with the CTFs pattern, the amount of Aβ was elevated in cells overexpressing FE65 or FE65 S610A but not in cells overexpressing FE65 S610D (Figure 4C). Next, the effect of SGK1 on Aβ generation was evaluated. As shown in Figure 4(D), SGK1-CA suppresses the FE65-mediated increase in Aβ generation. However, SGK1-CA has no significant effect on FE65 S610A-promoted Aβ level. This finding further supports that phosphorylation of FE65 at Ser^{610} by SGK1 abolishes the effect of FE65 on APP processing and Aβ liberation.

FE65 stabilizes APP holoprotein

We observed that the level of APP holoprotein is increased when FE65 or FE65 S610A was overexpressed in APP + BACE1 co-transfected cells, a phenomenon which is absent from APP + BACE1 + FE65 S610D co-transfected cells (Figure 4B). We hypothesized that FE65, through its interaction with APP, stabilizes APP holoprotein, rendering more substrates for β-secretase cleavage and thus enhances Aβ generation. To test this hypothesis, we performed a CHX chase assay to determine the half-life of APP in the absence or presence of FE65. The

© 2015 Authors; published by Portland Press Limited

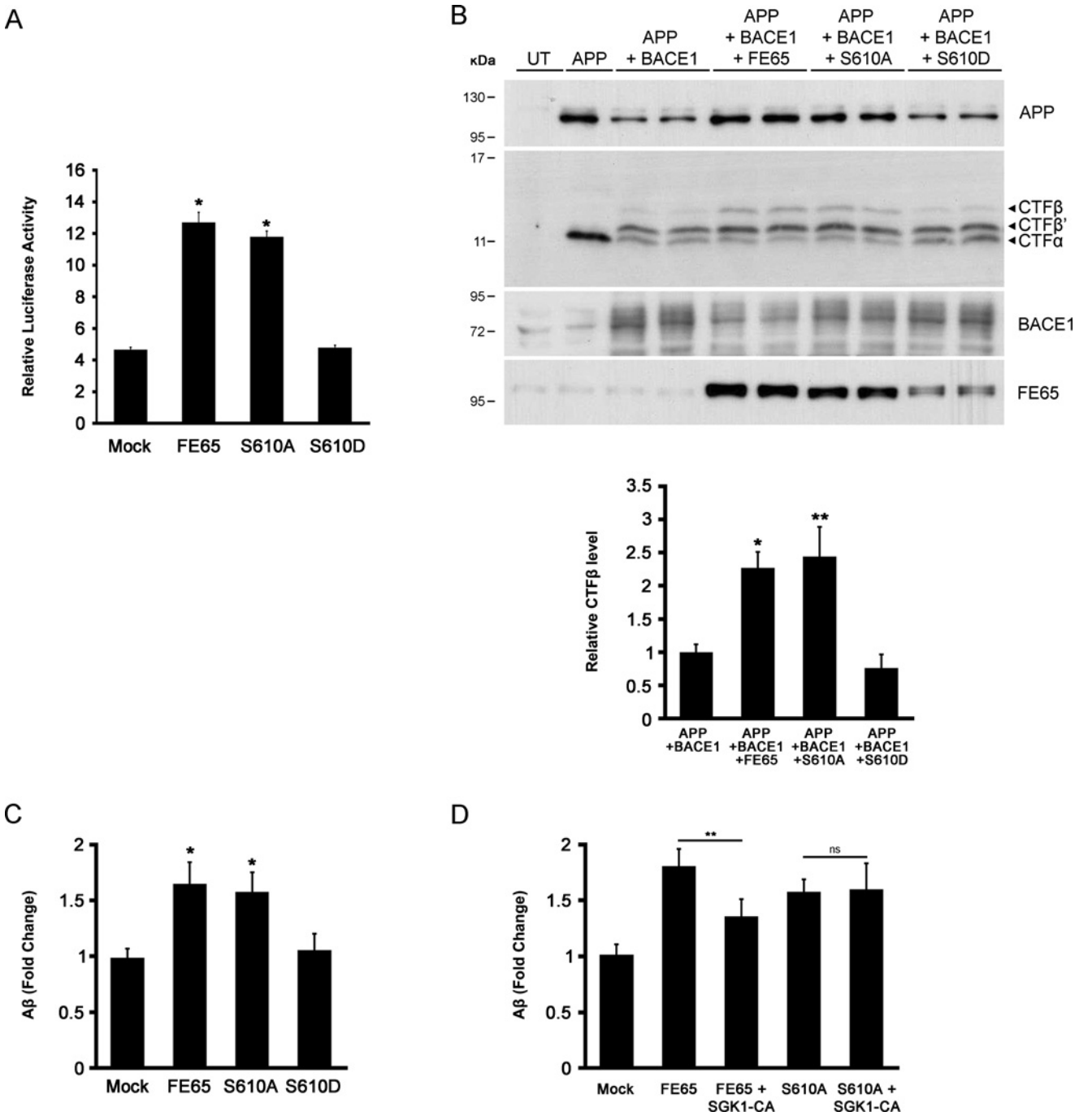

Figure 4 Phosphorylation of FE65 Ser^{610} abolishes the effect of FE65 on APP processing

(**A**) CHO cells were co-transfected with APP–GAL4, pFR-Luc and phRL-TK together with FE65/FE65 S610A/FE65 S610D. FE65 S610A shows a similar effect on APP–GAL4 cleavage as FE65 whereas FE65 S610D is unable to stimulate APP cleavage. $n = 5$. *$P < 0.0001$ compared with Mock. Results are means $\pm$ S.D. (**B**) CHO cells were co-transfected with APP + BACE1 + FE65/FE65 S610A/FE65 S610D. Forty-eight hours post-transfection, the transfected cell lysate was resolved on a 16 % Tris-tricine gel to analyse the amount of APP CTFα and CTFβ generated. The protein levels of APP holoprotein, BACE1 and FE65 were analysed by Western blotting. FE65 S610D shows reduced CTFβ generation. CTFβ levels were analysed by densitometry. Data for the graph were obtained from three independent experiments with $n = 3$ (total number of samples analysed = 9). *$P < 0.0001$; **$P < 0.01$ compared with APP + BACE1. Results are means $\pm$ S.D. (**C**) CHO cells were co-transfected with APP + Mock, FE65, FE65 S610A or FE65 S610D. Forty-eight hours post-transfection, cell culture medium were aspirated and changed to fresh medium. The level of secreted Aβ was assayed using ELISA kit 7 h after change of medium. $n = 5$. *$P < 0.0001$ compared with Mock. FE65 S610D does not enhance Aβ liberation. (**D**) CHO cells were co-transfected with APP + the indicated constructs and the level of secreted Aβ was assayed. $n = 5$. **$P < 0.01$; ns–$P > 0.05$. Results are means $\pm$ S.D. SGK1 suppresses FE65-enhanced Aβ liberation through phosphorylation of Ser^{610}.

© 2015 Authors; published by Portland Press Limited

transfected cells were treated with CHX, a protein synthesis inhibitor, 48 h post-transfection and the cells were subsequently chased at different time points of CHX treatment. Our result shows that in the presence of FE65, the half-life of APP is prolonged (Figures 5A and 5B). Previously, we and others showed that loss of FE65 results in proteins destabilization via the ubiquitin–proteasome system (UPS) [32,39]. We investigated whether FE65 stabilizes APP through preventing its degradation via UPS. To clarify this, proteasome inhibitor MG132 was added to APP + control or FE65 siRNA co-transfected cells and the protein level of APP was analysed by Western blotting. DMSO was used as a vehicle control. As shown in Figure 5(C), in control cells, FE65 knockdown leads to depletion of APP holoprotein level, which is in line with the CHX chase assay result (Figures 5A and 5B). When MG132 was added to the transfected cells, the depletion of APP upon FE65 knockdown was prevented. On the other hand, autophagy inhibitor 3-MA is unable to rescue the reduction in APP upon FE65 knockdown (Figure 5D). This suggests that loss of FE65 promotes APP degradation via UPS but not autophagy.

Phosphorylation status of Ser^{610} of FE65 regulates the turnover of APP

Next, we sought to determine the effect of FE65 Ser^{610} phosphorylation on the turnover of APP. The turnover rate of APP in the presence of FE65/FE65 S610A/FE65 S610D was compared by CHX chase assay followed by densitometric analysis (Figures 6A and 6B). Our data show that FE65 S610A but not FE65 S610D prolongs the half-life of APP. Of note, it was found that FE65 S610D shows a higher turnover rate than FE65 and FE65 S610A (Figures 6A and 6C). We asked whether APP plays a role in regulating FE65 turnover. To address this issue, cells transfected with FE65/FE65 S610A/FE65 S610D + control or APP siRNA were either treated with proteasome inhibitor MG132 or vehicle control (DMSO) and the protein level of FE65 was analysed by Western blotting. As shown in Figure 6(D), APP knockdown results in reduction in FE65 and FE65 S610A levels (lane 1 compared with lane 2; lane 5 compared with lane 6) and the depletion is blocked upon MG132 treatment (lane 3 compared with lane 4; lane 7 compared with lane 8). This indicates that APP stabilizes FE65 and FE65 S610A by preventing their degradation through UPS. On the other hand, the protein level of FE65 S610D, which is unable to bind to APP, is not affected by endogenous APP level (lane 9 compared with lane 10). In a complementary approach, we performed an MG132 study in APP + FE65/FE65 S610A/S610D-transfected cells to evaluate the effect of FE65 Ser^{610} phosphorylation on APP and FE65 proteasomal degradation. As shown in Figure 6(E), depletion of APP and FE65 in APP + FE65 S610D-transfected cells is rescued by proteasome inhibition by MG132. A previous report provided evidence that APP is ubiquitinated by the FBL2, a component of the SCF (Skp1–cullin1–F-box protein) E3 ubiquitin ligase complex, resulting in enhanced proteasomal degradation [40]. We enquired whether FE65 precludes FBL2-mediated APP degradation. To do this, cells were co-transfected with APP + FE65, FE65 S610A or FE65 S610D + control or FBL2 siRNA and APP protein level was compared. As shown in Figure 6(F), loss of FBL2 partially restores APP level in APP + FE65 S610D-transfected cells. Taken together, the current findings suggest that the interaction between APP and FE65 protects APP from proteasomal degradation through FBL2 and this process is regulated by the phosphorylation status of FE65 Ser^{610}.

In an attempt to evaluate the effect of SGK1 on APP turnover, CHX chase assay was performed in cells co-transfected with either APP + FE65 or APP + FE65 + SGK1-CA and the turnover rate of APP was compared by densitometric analysis (Figures 7A and 7B). SGK1 was found to shorten the half-life of APP and promote APP turnover. A similar experiment was performed in cells co-transfected with either APP + FE65 S610A or APP + FE65 S610A + SGK1-CA (Figures 7C and 7D) and APP + FE65 siRNA or APP + FE65 siRNA + SGK1-CA (Figures 7E and 7F). In the absence of phosphorylatable Ser^{610} or FE65, SGK1 is unable to enhance APP turnover, indicating that SGK1 promotes APP turnover through phosphorylation of FE65 at Ser^{610}.

DISCUSSION

Although it is long known that FE65 is a phosphoprotein, the importance of most of these phospho-residues remains unexplored [41–43]. In the present study, we demonstrated that phosphorylation of FE65 Ser^{610} by SGK1 attenuates the interaction between FE65 and APP (Figure 1). Our findings are similar to those of others who provided evidence that SGK1 phosphorylates a rat variant of FE65 [44]. FE65 Ser^{610} is located within the PTB2 domain of FE65, which is the domain that is responsible for APP binding. In fact, structural analysis of FE65 PTB2 domain in complex with AICD-C32$_{aa664-695}$ performed by Radzimanowski et al [34] revealed that Ser^{610} is involved the interaction interface. Our experimental data and MD simulation (Figure 2) further support the importance of FE65 Ser^{610} as a critical aa in APP–FE65 interaction and reveals a novel molecular mechanism that modulates APP–FE65 interaction.

It is known that AICD acts as a cytosolic docking site of FE65 and refrains FE65 from nuclear translocation. The cytosolic localization of FE65 has in fact important implications for its functions, in particular, the modulation of APP processing [45]. Being a multi-domain adaptor protein, FE65 has been reported to serve as a bridging molecule between the cytosolic tails of APP and a number of apolipoprotein E (ApoE) receptors including low-density lipoprotein receptor-related protein (LRP1), ApoER2 and very low-density lipoprotein receptor (VLDLR). Through the formation of these APP–FE65–ApoE receptors trimeric complexes, FE65 acts as a functional linker and mediates Aβ secretion [14,46–48]. In the present study, we showed that the co-localization of APP and FE65 in the perinuclear region is lost when FE65 Ser^{610} is phosphorylated and FE65 is retained in the nucleus (Figure 3). The disruption in APP–FE65 co-localization when FE65 Ser^{610} is phosphorylated hints at alteration of FE65-mediated APP processing. In this regard, we demonstrated that phosphorylation of FE65 Ser^{610} by SGK1 abolishes the effect of FE65 on APP processing and the amount of secreted Aβ is comparable to APP + Mock control (Figure 4). This is in agreement with a previous study conducted by Barbagallo et al. [49], which demonstrated that knockin mice carrying APP Y682G mutation, a mutant that does not bind FE65, exhibit a reduced Aβ level, indicating that Aβ secretion is dependent, at least in part, on APP–FE65 interaction.

An increasing body of evidence suggests that the regulation of APP holoprotein level is important for AD pathogenesis. First, triplication of the *APP* gene on chromosome 21 in Down's syndrome (DS) patients is associated with development of early onset AD [50,51]. On the other hand, in DS patients with only partial trisomy 21 that excludes *APP* gene, AD pathology was not observed even at an advanced age [52]. Second, APP mRNA level was reported to be elevated in sporadic AD, accompanied by a marked decrease in miR-106b, a negative regulator of APP expression [53,54]. Third, degradation of APP through the lysosomal pathway and proteasomal pathway has been implicated

© 2015 Authors; published by Portland Press Limited

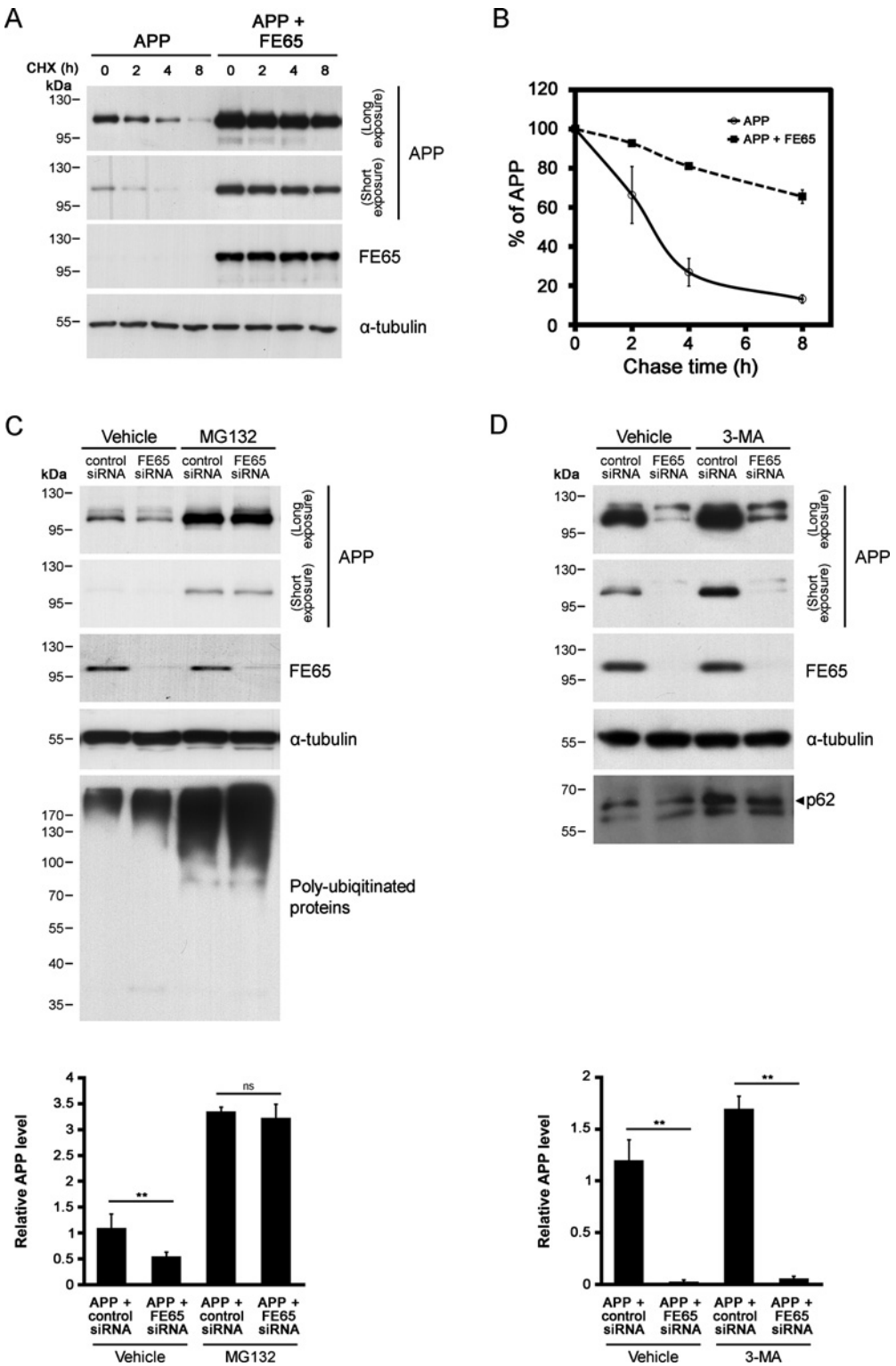

Figure 5 FE65 stabilizes APP holoprotein

(**A**) CHO cells transfected with the APP or APP + FE65 were subjected to 10 μg/ml CHX treatment 48 h post-transfection and chased for the indicated times. Cell lysates were analysed by Western blotting. (**B**) Densitometric analysis of APP levels that are shown in (**A**). Data were obtained from four independent experiments with $n = 5$ (total number of samples analysed was 20). Results are means $\pm$ S.E.M. Cells co-transfected with APP + control or FE65 siRNA were incubated with (**C**) 2.5 μM MG132 or DMSO vehicle for 16 h and (**D**) 5 mM 3-MA or vehicle control for 12 h. The protein levels of APP in transfected cell lysates were compared by Western blotting. APP levels in (**C**) and (**D**) were obtained from three independent experiments ($n = 3$). $^{**}P < 0.01$; ns–$P > 0.05$. Results are means $\pm$ S.D. FE65 knockdown-mediated reduction in APP levels is blocked by MG132 but not 3-MA.

© 2015 Authors; published by Portland Press Limited

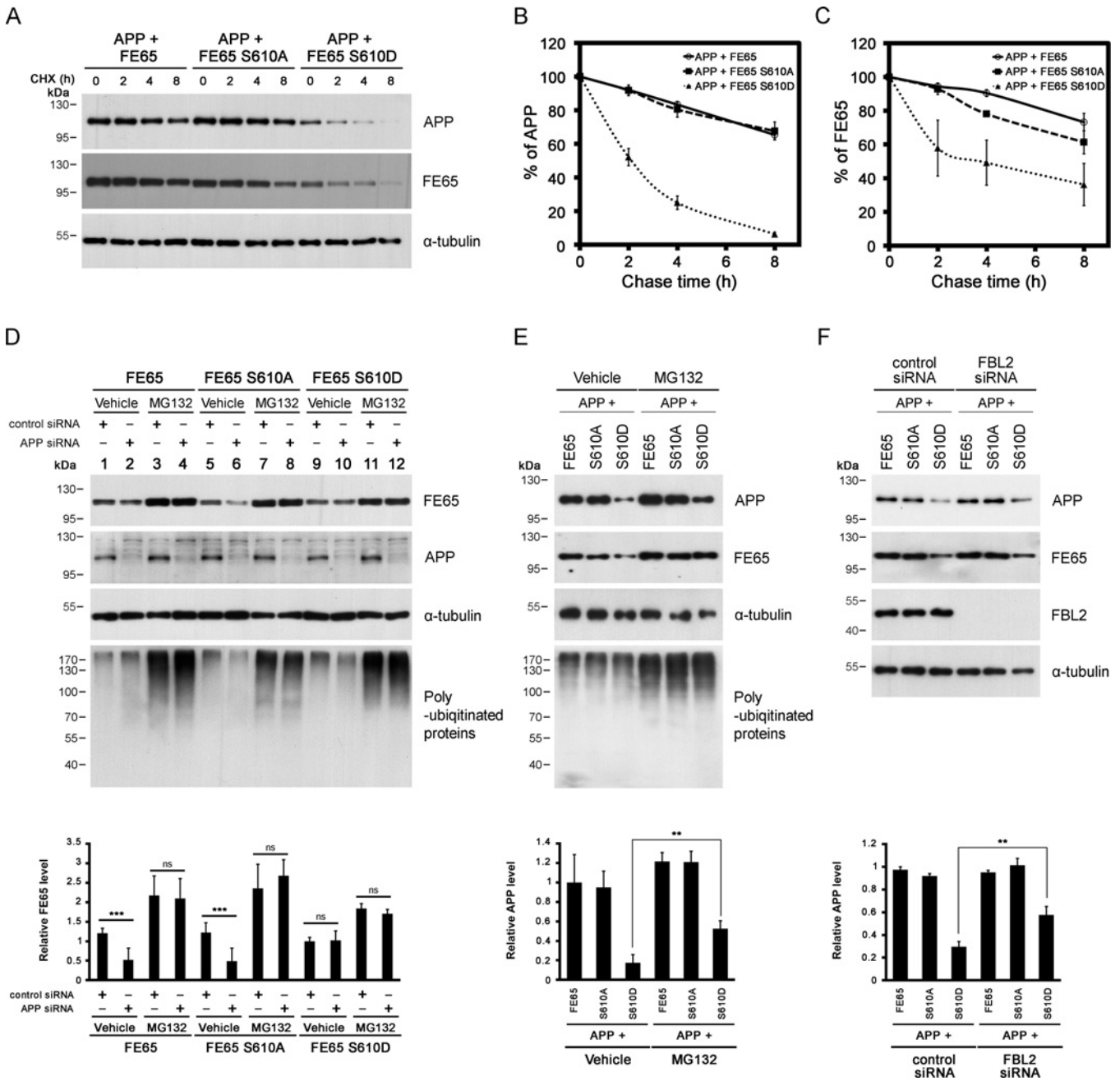

Figure 6 Phosphorylation status of FE65 Ser^{610} regulates APP and FE65 turnover

(**A**) CHX chase assay was performed on cells transfected with APP + FE65, FE65 S610A or FE65 S610D. Cell lysates were immunoblotted for APP, FE65 and α-tubulin. (**B** and **C**) Densitometric analysis of APP and FE65 levels that are shown in (**A**). FE65 and APP levels were obtained from four independent experiments with $n = 5$ (total number of samples analysed was 20). Results are means $\pm$ S.E.M. FE65 S610A but not S610D prolongs the half-life of APP. (**D**) Cells co-transfected with FE65, FE65 S610A or FE65 S610D + control or APP siRNA were incubated with 2.5 μM MG132 or DMSO vehicle for 16 h. APP knockdown-mediated reduction in FE65 and FE65 S610A levels is rescued by MG132. Protein level of FE65 S610D is unaffected by APP knockdown. (**E**) Cells co-transfected with APP + FE65, FE65 S610A or FE65 S610D were subjected to 16 h MG132 treatment. The protein levels of APP and FE65 in transfected cell lysates was compared by Western blotting. Accelerated APP and FE65 turnover in APP + FE65 S610D-transfected cells is rescued by MG132. (**F**) Cells were co-transfected with APP + FE65, FE65 S610A or FE65 S610D + control or FBL2 siRNA. The transfected cell lysate was immunoblotted for APP, FE65 and FBL2. FBL2 knockdown partially restores APP level in APP + FE65 S610D-transfected cells. Data for graphs in (**D**–**F**) were obtained from three independent experiments with $n = 3$ (total number of samples analysed = 9) and analysed by one-way ANOVA. $^{**}P < 0.01$; $^{***}P < 0.05$; ns–$P > 0.05$. Results are means $\pm$ S.D.

in reduction in Aβ liberation [40,55–58]. We presented here for the first time that FE65 stabilizes APP holoprotein and prolongs its half-life by preventing APP degradation through UPS (Figure 5). Previously, we and an other group have demonstrated that FE65 stabilizes p53 and huntingtin (Htt) by suppressing their degradation through UPS [32,39]. The current finding has two important implications: (1) it reinforces the role of FE65 as a negative regulator in UPS-mediated degradation and (2) other than acting as a bridging molecule between APP and ApoE receptors, such as LRP1, ApoER2 and VLDLR, which modulate APP

© 2015 Authors; published by Portland Press Limited

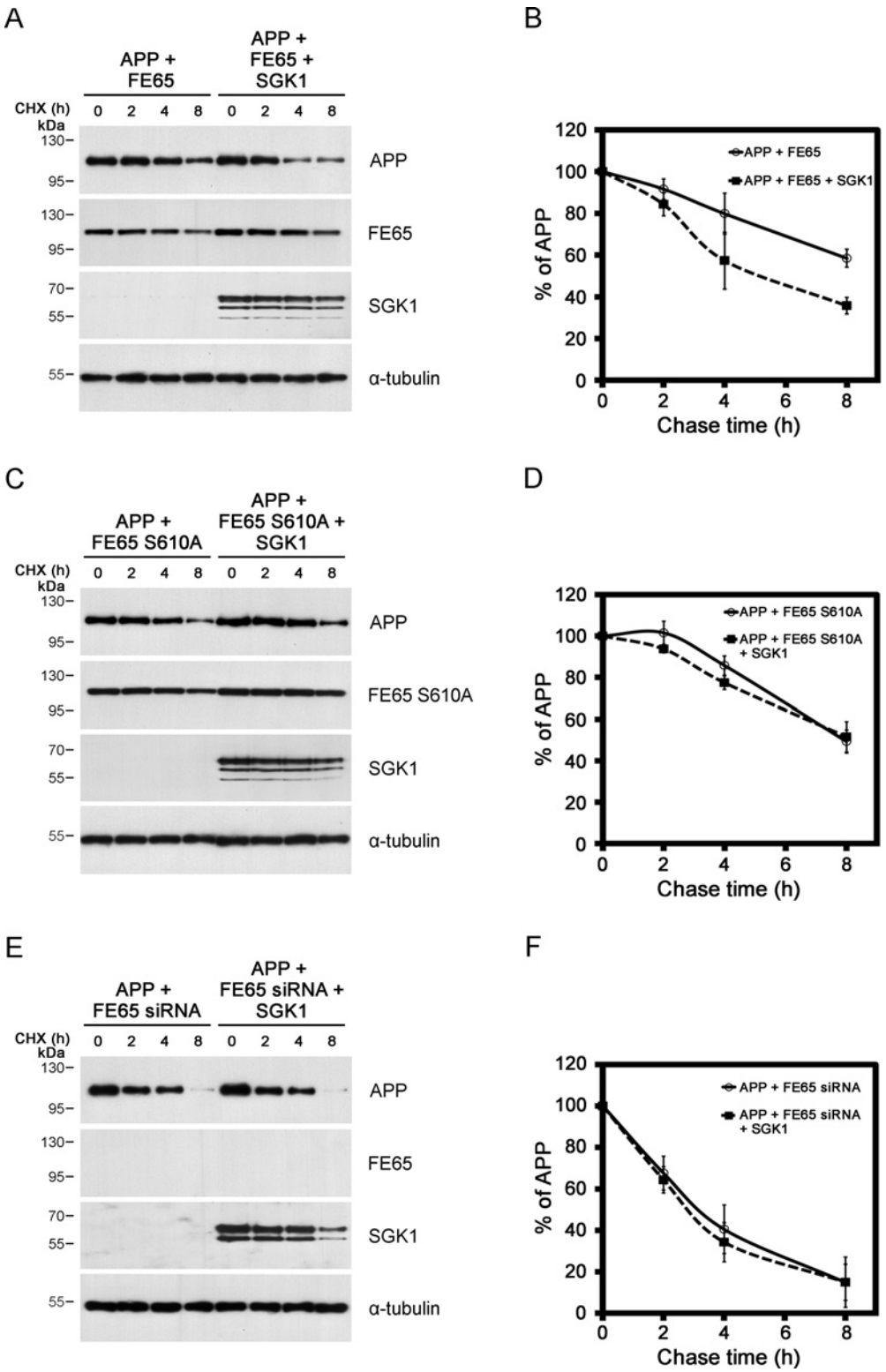

Figure 7 Effect of SGK1 on APP turnover

Cells transfected with (**A**) APP + FE65 or APP + FE65 + SGK1-CA, (**C**) APP + FE65 S610A or APP + FE65 S610A + SGK1-CA and (**E**) APP + FE65 siRNA or APP + FE65 siRNA + SGK1-CA were subjected to 10 μg/ml CHX treatment 48 h post-transfection and chased for the indicated times. Cell lysates were analysed by Western blotting. (**B**, **D** and **F**) Densitometric analysis of APP levels that are shown in (**A**, **C** and **E**) respectively. Data were obtained from four independent experiments with $n = 5$ (total number of samples analysed was 20). Results are means $\pm$ S.E.M.

© 2015 Authors; published by Portland Press Limited

processing, FE65 serves to suppress APP holoprotein turnover through UPS, thereby enhancing Aβ generation [14,46–48].

Importantly, the phosphorylation status of FE65 Ser^{610} was shown to regulate the turnover rate of APP. Consistent with the interaction behaviour, phosphorylation of FE65 Ser^{610} abrogates the stabilization effect on APP, leading to a shorter half-life (Figures 6A, 6B and 6E). This provides a mechanistic explanation of the regulatory effect of FE65 Ser^{610} phosphorylation on APP processing. Additionally, we provided evidence that degradation of FE65 and FE65 S610A through UPS is suppressed by APP, a phenomenon which is not observed in FE65 S610D (Figures 6C and 6D). Several studies showed that APP can be targeted to proteasome through multiple pathways, leading to reduction in Aβ generation. For instance, APP was reported to be an endoplasmic reticulum-associated degradation (ERAD) substrate where it is ubiquitinated by ER-localized E3 ubiquitin ligase HRD1 and the stress-responsive chaperone-protease HtrA2, through binding to the N-terminal region of APP, serves as a shuttling chaperone to assist proteasome targeting [55,56]. In the present study, we showed that knockdown of FBL2, a component of a reported APP E3 ubiquitin ligase which is primarily found in ER, partially rescues accelerated APP degradation in FE65 S610D-transfected cells (Figure 6F). A previous report indicated that APP and FE65 interact in various subcellular compartments along the secretory pathway including ER as evidenced by subcellular fractionation by iodixanol gradients [8]. It is therefore possible that FE65 competes with FBL2 for APP binding in ER, thereby preventing APP proteasomal degradation and promotes Aβ generation. However, further investigation on the underlying mechanism by which FE65 blocks APP degradation through UPS is clearly warranted. In particular, the ubiquitination level of APP in the presence or absence of FE65 should be evaluated. On the other hand, it is worthwhile to investigate whether or not APP–FE65 interaction prevents FBL2 from accessing APP. Nevertheless, our current finding underscores the importance of APP–FE65 interaction in regulating the metabolic turnover of APP through UPS, which in turn modulates APP processing and thus Aβ generation.

Furthermore, in the present study, we demonstrated that SGK1 attenuates APP–FE65 interaction through FE65 Ser^{610} phosphorylation (Figure 1), suppresses FE65-enhanced Aβ secretion (Figure 4D) and promotes APP turnover through phosphorylating FE65 (Figure 7). SGK1 is a serine/threonine kinase downstream of the phosphatidylinositol 3-kinase (PI3K) cascade and its expression is acutely regulated by serum and glucocorticoids [36,59]. It is known to shuttle between nucleus and cytosol and localize to ER under certain circumstances [60–62]. In our study, we propose that (1) FE65 binds to APP holoprotein and prevents proteasomal degradation of APP, presumably in ER and (2) SGK1 phosphorylates FE65 Ser^{610} and abrogates the interaction between APP and FE65. Since both FE65 and SGK1 shuttle between nucleus and cytosol, there are two possible scenarios concerning the phosphorylation event.

(1) SGK1 phosphorylates FE65 in the cytosol before FE65 binds to APP and thereby blocks APP–FE65 interaction.

(2) SGK1 phosphorylates FE65 in the ER when it is bound to APP and serves as a dissociation signal of APP–FE65 interaction.

In either scenario, phosphorylation of FE65 by SGK1 attenuates APP–FE65 interaction and APP becomes more prone to proteasomal degradation. Additionally, SGK1 has been previously shown to phosphorylate the γ-secretase component nicastrin (NCT) and promote its degradation [63]. Examination of APP, CTFs and AICD protein levels and activity of C99-GAL4/VP16 luciferase reporter revealed that γ-secretase-mediated APP cleavage is suppressed by SGK1. Our work demonstrated for the first time that SGK1, through phosphorylating FE65 Ser^{610}, modulates Aβ liberation (Figure 4D) and unravelled a novel pathway by which SGK1 regulates APP processing. Intriguingly, transforming growth factor β (TGFβ), a powerful stimulator of SGK1, is known to confer a neuroprotective effect against Aβ [64]. In this regard, an attempt has been made to search for small molecule TGFβ mimetics as potential AD therapeutic candidates [65]. It is hoped that through identifying a specific stimulator of SGK1, more potential candidates for future AD drug design could be developed.

In conclusion, we found that FE65 enhances APP processing and Aβ generation by preventing APP holoprotein degradation. Importantly, phosphorylation of FE65 Ser^{610} by SGK1 acts as a molecular switch of this event. Our findings shed light on the dual role of SGK1 in reducing APP processing and potentially delaying AD pathogenesis. Future studies on the level of SGK1 and FE65 Ser^{610} phosphorylation in AD compared with control brains would provide valuable information on AD pathology.

AUTHOR CONTRIBUTION

Vanessa Chow, Jacky Ngo, Wen Li, Yu Wai Chen, Vincent Tam, Edwin Chan, Christopher Miller and Kwok-Fai Lau conceived the study and designed the experiments. Vanessa Chow, Jacky Ngo, Wen Li and Vincent Tam performed the experiments. Vanessa Chow, Jacky Ngo, Wen Li, Yu Wai Chen, Vincent Tam, Edwin Chan, Christopher Miller and Kwok-Fai Lau analysed the data and wrote the paper.

ACKNOWLEDGEMENTS

We thank David Pearce for mammalian expression SGK1 construct.

FUNDING

This work was supported by the Health and Medical Research Fund (Hong Kong) [grant number 01120196]; the Research Grants Council Hong Kong [grant number CUHK 467712]; the CUHK direct grant scheme [grant numbers 4053102 and 4053045]; the Alzheimer's Research UK [grant number ARUK-PhD-2012-1]; and Wellcome Trust [grant number WT078662].

REFERENCES

1 Wimo, A. and Prince, M. (2010) World Alzheimer Report 2010: The Global Economic Impact of Dementia, Alzheimer's Disease International
2 O'Brien, R.J. and Wong, P.C. (2011) Amyloid precursor protein processing and Alzheimer's disease. Annu. Rev. Neurosci. **34**, 185–204 CrossRef PubMed
3 McLoughlin, D.M. and Miller, C.C. (2008) The FE65 proteins and Alzheimer's disease. J. Neurosci. Res. **86**, 744–754 CrossRef PubMed
4 Tang, B.L. and Liou, Y.C. (2007) Novel modulators of amyloid-beta precursor protein processing. J. Neurochem. **100**, 314–323 CrossRef PubMed
5 Buoso, E., Lanni, C., Schettini, G., Govoni, S. and Racchi, M. (2010) βAmyloid precursor protein metabolism: focus on the functions and degradation of its intracellular domain. Pharmacol. Res. **62**, 308–317 CrossRef PubMed
6 Kesavapany, S., Banner, S.J., Lau, K.F., Shaw, C.E., Miller, C.C., Cooper, J.D. and McLoughlin, D.M. (2002) Expression of the Fe65 adapter protein in adult and developing mouse brain. Neuroscience **115**, 951–960 CrossRef PubMed
7 Pardossi-Piquard, R. and Checler, F. (2012) The physiology of the beta-amyloid precursor protein intracellular domain AICD. J. Neurochem. **120** (Suppl 1), 109–124 CrossRef PubMed
8 Sabo, S.L., Lanier, L.M., Ikin, A.F., Khorkova, O., Sahasrabudhe, S., Greengard, P. and Buxbaum, J.D. (1999) Regulation of beta-amyloid secretion by FE65, an amyloid protein precursor-binding protein. J. Biol. Chem. **274**, 7952–7957 CrossRef PubMed
9 Ando, K., Iijima, K.I., Elliott, J.I., Kirino, Y. and Suzuki, T. (2001) Phosphorylation-dependent regulation of the interaction of amyloid precursor protein with Fe65 affects the production of beta-amyloid. J. Biol. Chem. **276**, 40353–40361 CrossRef PubMed

© 2015 Authors; published by Portland Press Limited

10 Wang, B., Hu, Q., Hearn, M.G., Shimizu, K., Ware, C.B., Liggitt, D.H., Jin, L.W., Cool, B.H., Storm, D.R. and Martin, G.M. (2004) Isoform-specific knockout of FE65 leads to impaired learning and memory. J. Neurosci. Res. **75**, 12–24 CrossRef PubMed

11 Guenette, S., Chang, Y., Hiesberger, T., Richardson, J.A., Eckman, C.B., Eckman, E.A., Hammer, R.E. and Herz, J. (2006) Essential roles for the FE65 amyloid precursor protein-interacting proteins in brain development. EMBO J. **25**, 420–431 CrossRef PubMed

12 Wiley, J.C., Smith, E.A., Hudson, M.P., Ladiges, W.C. and Bothwell, M. (2007) Fe65 stimulates proteolytic liberation of the beta-amyloid precursor protein intracellular domain. J. Biol. Chem. **282**, 33313–33325 CrossRef PubMed

13 Suh, J., Lyckman, A., Wang, L., Eckman, E.A. and Guenette, S.Y. (2011) FE65 proteins regulate NMDA receptor activation-induced amyloid precursor protein processing. J. Neurochem. **119**, 377–388 CrossRef PubMed

14 Dumanis, S.B., Chamberlain, K.A., Sohn, Y.J., Lee, Y.J., Guenette, S.Y., Suzuki, T., Mathews, P.M., Pak, D.T., Rebeck, G.W., Suh, Y.H. et al. (2012) FE65 as a link between VLDLR and APP to regulate their trafficking and processing. Mol. Neurodegener **7**, 9 CrossRef PubMed

15 Santiard-Baron, D., Langui, D., Delehedde, M., Delatour, B., Schombert, B., Touchet, N., Tremp, G., Paul, M.F., Blanchard, V., Sergeant, N. et al. (2005) Expression of human FE65 in amyloid precursor protein transgenic mice is associated with a reduction in beta-amyloid load. J. Neurochem. **93**, 330–338 CrossRef PubMed

16 Lau, K.F., Chan, W.M., Perkinton, M.S., Tudor, E.L., Chang, R.C., Chan, H.Y., McLoughlin, D.M. and Miller, C.C. (2008) Dexras1 interacts with FE65 to regulate FE65-amyloid precursor protein-dependent transcription. J. Biol. Chem. **283**, 34728–34737 CrossRef PubMed

17 Jowsey, P.A. and Blain, P.G. (2014) Fe65 Ser228 is phosphorylated by ATM/ATR and inhibits Fe65-APP-mediated gene transcription. Biochem. J. **465**, 413–421 CrossRef

18 Lau, K.F., McLoughlin, D.M., Standen, C.L., Irving, N.G. and Miller, C.C. (2000) Fe65 and X11beta co-localize with and compete for binding to the amyloid precursor protein. Neuroreport **11**, 3607–3610 CrossRef PubMed

19 Perkinton, M.S., Standen, C.L., Lau, K.F., Kesavapany, S., Byers, H.L., Ward, M., McLoughlin, D.M. and Miller, C.C. (2004) The c-Abl tyrosine kinase phosphorylates the Fe65 adaptor protein to stimulate Fe65/amyloid precursor protein nuclear signaling. J. Biol. Chem. **279**, 22084–22091 CrossRef PubMed

20 Angeletti, B., Waldron, K.J., Freeman, K.B., Bawagan, H., Hussain, I., Miller, C.C., Lau, K.F., Tennant, M.E., Dennison, C., Robinson, N.J. and Dingwall, C. (2005) BACE1 cytoplasmic domain interacts with the copper chaperone for superoxide dismutase-1 and binds copper. J. Biol. Chem. **280**, 17930–17937 CrossRef PubMed

21 Zambrano, N., Gianni, D., Bruni, P., Passaro, F., Telese, F. and Russo, T. (2004) Fe65 is not involved in the platelet-derived growth factor-induced processing of Alzheimer's amyloid precursor protein, which activates its caspase-directed cleavage. J. Biol. Chem. **279**, 16161–16169 CrossRef PubMed

22 Lau, K.F., McLoughlin, D.M., Standen, C. and Miller, C.C. (2000) X11 alpha and x11 beta interact with presenilin-1 via their PDZ domains. Mol. Cell Neurosci. **16**, 557–565 CrossRef PubMed

23 Hao, Y., Perkinton, M.S., Chan, W.W., Chan, H.Y., Miller, C.C. and Lau, K.F. (2011) GULP1 is a novel APP-interacting protein that alters APP processing. Biochem. J. **436**, 631–639 CrossRef PubMed

24 Emsley, P., Lohkamp, B., Scott, W.G. and Cowtan, K. (2010) Features and development of Coot. Acta Crystallogr. D. Biol. Crystallogr. **66**, 486–501 CrossRef PubMed

25 Lovell, S.C., Word, J.M., Richardson, J.S. and Richardson, D.C. (2000) The penultimate rotamer library. Proteins **40**, 389–408 CrossRef PubMed

26 Nagata, K., Randall, A. and Baldi, P. (2014) Incorporating post-translational modifications and unnatural amino acids into high-throughput modeling of protein structures. Bioinformatics **30**, 1681–1689 CrossRef PubMed

27 Pronk, S., Pall, S., Schulz, R., Larsson, P., Bjelkmar, P., Apostolov, R., Shirts, M.R., Smith, J. C., Kasson, P.M., van der Spoel, D. et al. (2013) GROMACS 4.5: a high-throughput and highly parallel open source molecular simulation toolkit. Bioinformatics **29**, 845–854 CrossRef PubMed

28 Petrov, D., Margreitter, C., Grandits, M., Oostenbrink, C. and Zagrovic, B. (2013) A systematic framework for molecular dynamics simulations of protein post-translational modifications. PLoS Comput. Biol. **9**, e1003154 CrossRef PubMed

29 Margreitter, C., Petrov, D. and Zagrovic, B. (2013) Vienna-PTM web server: a toolkit for MD simulations of protein post-translational modifications. Nucleic Acids Res. **41**, W422–W426 CrossRef PubMed

30 Hess, B., Bekker, H., Berendsen, H.J.C. and Fraaije, J.G.E.M. (1997) LINCS: a linear constraint solver for molecular simulations. J. Comput. Chem. **18**, 1463–1472 CrossRef

31 Humphrey, W., Dalke, A. and Schulten, K. (1996) VMD: visual molecular dynamics. J. Mol. Graph. **14**, 33–38 CrossRef PubMed

32 Chow, W.N., Luk, H.W., Chan, H.Y. and Lau, K.F. (2012) Degradation of mutant huntingtin via the ubiquitin/proteasome system is modulated by FE65. Biochem. J. **443**, 681–689 CrossRef PubMed

33 Lee, J.H., Lau, K.F., Perkinton, M.S., Standen, C.L., Rogelj, B., Falinska, A., McLoughlin, D.M. and Miller, C.C. (2004) The neuronal adaptor protein X11beta reduces amyloid beta-protein levels and amyloid plaque formation in the brains of transgenic mice. J. Biol. Chem. **279**, 49099–49104 CrossRef PubMed

34 Radzimanowski, J., Simon, B., Sattler, M., Beyreuther, K., Sinning, I. and Wild, K. (2008) Structure of the intracellular domain of the amyloid precursor protein in complex with Fe65-PTB2. EMBO Rep. **9**, 1134–1140 CrossRef PubMed

35 Rigbolt, K.T., Prokhorova, T.A., Akimov, V., Henningsen, J., Johansen, P.T., Kratchmarova, I., Kassem, M., Mann, M., Olsen, J.V. and Blagoev, B. (2011) System-wide temporal characterization of the proteome and phosphoproteome of human embryonic stem cell differentiation. Sci. Signal. **4**, rs3 CrossRef PubMed

36 Kobayashi, T., Deak, M., Morrice, N. and Cohen, P. (1999) Characterization of the structure and regulation of two novel isoforms of serum- and glucocorticoid-induced protein kinase. Biochem. J. **344** Pt 1, 189–197 CrossRef PubMed

37 Yaffe, M.B., Leparc, G.G., Lai, J., Obata, T., Volinia, S. and Cantley, L.C. (2001) A motif-based profile scanning approach for genome-wide prediction of signaling pathways. Nat. Biotechnol. **19**, 348–353 CrossRef PubMed

38 Minopoli, G., de Candia, P., Bonetti, A., Faraonio, R., Zambrano, N. and Russo, T. (2001) The beta-amyloid precursor protein functions as a cytosolic anchoring site that prevents Fe65 nuclear translocation. J. Biol. Chem. **276**, 6545–6550 CrossRef PubMed

39 Nakaya, T., Kawai, T. and Suzuki, T. (2009) Metabolic stabilization of p53 by FE65 in the nuclear matrix of osmotically stressed cells. FEBS J. **276**, 6364–6374 CrossRef PubMed

40 Watanabe, T., Hikichi, Y., Willuweit, A., Shintani, Y. and Horiguchi, T. (2012) FBL2 regulates amyloid precursor protein (APP) metabolism by promoting ubiquitination-dependent APP degradation and inhibition of APP endocytosis. J. Neurosci. **32**, 3352–3365 CrossRef PubMed

41 Standen, C.L., Perkinton, M.S., Byers, H.L., Kesavapany, S., Lau, K.F., Ward, M., McLoughlin, D. and Miller, C.C. (2003) The neuronal adaptor protein Fe65 is phosphorylated by mitogen-activated protein kinase (ERK1/2). Mol. Cell Neurosci. **24**, 851–857 CrossRef PubMed

42 Huttlin, E.L., Jedrychowski, M.P., Elias, J.E., Goswami, T., Rad, R., Beausoleil, S.A., Villen, J., Haas, W., Sowa, M.E. and Gygi, S.P. (2010) A tissue-specific atlas of mouse protein phosphorylation and expression. Cell **143**, 1174–1189 CrossRef PubMed

43 Tweedie-Cullen, R.Y., Reck, J.M. and Mansuy, I.M. (2009) Comprehensive mapping of post-translational modifications on synaptic, nuclear, and histone proteins in the adult mouse brain. J. Proteome. Res. **8**, 4966–4982 CrossRef PubMed

44 Lee, E.J., Chun, J., Hyun, S., Ahn, H.R., Jeong, J.M., Hong, S.K., Hong, J.T., Chang, I.K., Jeon, H.Y., Han, Y.S. et al. (2008) Regulation Fe65 localization to the nucleus by SGK1 phosphorylation of its Ser566 residue. BMB Rep. **41**, 41–47 CrossRef PubMed

45 Borquez, D.A. and Gonzalez-Billault, C. (2012) The amyloid precursor protein intracellular domain-fe65 multiprotein complexes: a challenge to the amyloid hypothesis for Alzheimer's disease? Int. J. Alzheimers Dis. **2012**, 353145 PubMed

46 Pietrzik, C.U., Yoon, I.S., Jaeger, S., Busse, T., Weggen, S. and Koo, E.H. (2004) FE65 constitutes the functional link between the low-density lipoprotein receptor-related protein and the amyloid precursor protein. J. Neurosci. **24**, 4259–4265 CrossRef PubMed

47 Wagner, T. and Pietrzik, C.U. (2012) The role of lipoprotein receptors on the physiological function of APP. Exp. Brain Res. **217**, 377–387 CrossRef PubMed

48 Hoe, H.S., Magill, L.A., Guenette, S., Fu, Z., Vicini, S. and Rebeck, G.W. (2006) FE65 interaction with the ApoE receptor ApoEr2. J. Biol. Chem. **281**, 24521–24530 CrossRef PubMed

49 Barbagallo, A.P., Weldon, R., Tamayev, R., Zhou, D., Giliberto, L., Foreman, O. and D'Adamio, L. (2010) Tyr(682) in the intracellular domain of APP regulates amyloidogenic APP processing *in vivo*. PLoS One **5**, e15503 CrossRef PubMed

50 Rumble, B., Retallack, R., Hilbich, C., Simms, G., Multhaup, G., Martins, R., Hockey, A., Montgomery, P., Beyreuther, K. and Masters, C.L. (1989) Amyloid A4 protein and its precursor in Down's syndrome and Alzheimer's disease. N. Engl. J. Med. **320**, 1446–1452 CrossRef PubMed

51 Lott, I.T. and Head, E. (2005) Alzheimer disease and Down syndrome: factors in pathogenesis. Neurobiol. Aging **26**, 383–389 CrossRef PubMed

52 Millan Sanchez, M., Heyn, S.N., Das, D., Moghadam, S., Martin, K.J. and Salehi, A. (2012) Neurobiological elements of cognitive dysfunction in down syndrome: exploring the role of APP. Biol. Psychiatry **71**, 403–409 CrossRef PubMed

53 Matsui, T., Ingelsson, M., Fukumoto, H., Ramasamy, K., Kowa, H., Frosch, M.P., Irizarry, M.C. and Hyman, B.T. (2007) Expression of APP pathway mRNAs and proteins in Alzheimer's disease. Brain Res. **1161**, 116–123 CrossRef PubMed

54 Hebert, S.S., Horre, K., Nicolai, L., Bergmans, B., Papadopoulou, A.S., Delacourte, A. and De Strooper, B. (2009) MicroRNA regulation of Alzheimer's Amyloid precursor protein expression. Neurobiol. Dis. **33**, 422–428 CrossRef PubMed

55 Huttunen, H.J., Guenette, S.Y., Peach, C., Greco, C., Xia, W., Kim, D.Y., Barren, C., Tanzi, R.E. and Kovacs, D.M. (2007) HtrA2 regulates beta-amyloid precursor protein (APP) metabolism through endoplasmic reticulum-associated degradation. J. Biol. Chem. **282**, 28285–28295 CrossRef PubMed

56 Kaneko, M., Koike, H., Saito, R., Kitamura, Y., Okuma, Y. and Nomura, Y. (2010) Loss of HRD1-mediated protein degradation causes amyloid precursor protein accumulation and amyloid-beta generation. J. Neurosci. **30**, 3924–3932 CrossRef PubMed

57 Page, R.M., Munch, A., Horn, T., Kuhn, P.H., Colombo, A., Reiner, O., Boutros, M., Steiner, H., Lichtenthaler, S.F. and Haass, C. (2012) Loss of PAFAH1B2 reduces amyloid-beta generation by promoting the degradation of amyloid precursor protein C-terminal fragments. J. Neurosci. **32**, 18204–18214 CrossRef PubMed

© 2015 Authors; published by Portland Press Limited

58 Yang, Y., Wu, Y., Zhang, S. and Song, W. (2013) High glucose promotes Abeta production by inhibiting APP degradation. PLoS One **8**, e69824 CrossRef PubMed
59 Webster, M.K., Goya, L., Ge, Y., Maiyar, A.C. and Firestone, G.L. (1993) Characterization of sgk, a novel member of the serine/threonine protein kinase gene family which is transcriptionally induced by glucocorticoids and serum. Mol. Cell Biol. **13**, 2031–2040 PubMed
60 Buse, P., Tran, S.H., Luther, E., Phu, P.T., Aponte, G.W. and Firestone, G.L. (1999) Cell cycle and hormonal control of nuclear-cytoplasmic localization of the serum- and glucocorticoid-inducible protein kinase, Sgk, in mammary tumor cells. A novel convergence point of anti-proliferative and proliferative cell signaling pathways. J. Biol. Chem. **274**, 7253–7263 CrossRef PubMed
61 Alliston, T.N., Gonzalez-Robayna, I.J., Buse, P., Firestone, G.L. and Richards, J.S. (2000) Expression and localization of serum/glucocorticoid-induced kinase in the rat ovary: relation to follicular growth and differentiation. Endocrinology **141**, 385–395 PubMed
62 Arteaga, M.F., Wang, L., Ravid, T., Hochstrasser, M. and Canessa, C.M. (2006) An amphipathic helix targets serum and glucocorticoid-induced kinase 1 to the endoplasmic reticulum-associated ubiquitin-conjugation machinery. Proc. Natl. Acad. Sci. U.S.A. **103**, 11178–11183 CrossRef PubMed
63 Mo, J.S., Yoon, J.H., Hong, J.A., Kim, M.Y., Ann, E.J., Ahn, J.S., Kim, S.M., Baek, H.J., Lang, F., Choi, E.J. and Park, H.S. (2012) Phosphorylation of nicastrin by SGK1 leads to its degradation through lysosomal and proteasomal pathways. PLoS One **7**, e37111 CrossRef PubMed
64 Lang, F., Strutz-Seebohm, N., Seebohm, G. and Lang, U.E. (2010) Significance of SGK1 in the regulation of neuronal function. J. Physiol. **588**, 3349–3354 CrossRef PubMed
65 Zhang, H., Zou, K., Tesseur, I. and Wyss-Coray, T. (2005) Small molecule tgf-beta mimetics as potential neuroprotective factors. Curr. Alzheimer Res. **2**, 183–186 CrossRef PubMed

Received 9 December 2014/17 July 2015; accepted 17 July 2015
Accepted Manuscript online 17 July 2015, doi:10.1042/BJ20141485

© 2015 Authors; published by Portland Press Limited